

To appear in A.J., June 1977

## A Correlation between Balmer H $\alpha$ Emission and Infrared Cirrus

Peter R. McCullough<sup>1</sup>

Astronomy Department, University of Illinois, Urbana, IL, 61801

### ABSTRACT

A  $13^\circ \times 13^\circ$  image of Balmer H $\alpha$  emission at galactic latitude  $-65^\circ$  is presented. Sensitivity is limited in part by confusion<sup>2</sup>: the peak-to-valley anisotropy of the H $\alpha$  surface brightness is  $\sim 0.2$  Rayleighs on angular scales of  $0.1^\circ$  to  $1.0^\circ$ . The morphology of the H $\alpha$  emission is similar to that of the  $100 \mu\text{m}$  emission previously observed by the Infrared Astronomical Satellite (IRAS). A point-by-point comparison of the two shows a marginally detected ( $3\sigma$ ) positive correlation,  $\rho = +0.14 \pm 0.04$ . The slope of the correlated components of the  $100 \mu\text{m}$  and H $\alpha$  emissions is  $1.26^{+0.45}_{-0.32} \text{ MJy sr}^{-1} \text{ R}^{-1}$ . Using parameters from the literature, we predict that emission from dust and ionized gas at high latitudes produces  $\sim 3$  times more H $\alpha$  emission per unit  $100 \mu\text{m}$  emission than does backscattering of H $\alpha$  emission from Galactic H II regions by dust at high latitude. Observations of this type may allow us to distinguish between Galactic foreground and cosmic background for both the free-free emission and the thermal dust emission associated with the warm ionized medium of the Milky Way.

*Subject headings:*

### 1. Introduction

Martin Harwit (Harwit 1981) might say we have rediscovered in H $\alpha$  the interstellar cirrus that was discovered first in the infrared by IRAS (Lo et al. 1984). Such a rediscovery is not insignificant.

To measure anisotropy of the cosmic microwave background, astronomers must first measure and subtract foreground emission from the Milky Way's interstellar medium (ISM). Three

---

<sup>1</sup>Alfred P. Sloan Research Fellow.

<sup>2</sup>The H $\alpha$  surface brightness at high Galactic latitudes is approximately 1 Rayleigh (R), where  $1 \text{ R} = 10^6/4\pi \text{ photons cm}^{-2} \text{ s}^{-1} \text{ sr}^{-1}$  (Reynolds 1992). At H $\alpha$   $1 \text{ R} = 2.42 \times 10^{-7} \text{ ergs cm}^{-2} \text{ s}^{-1} \text{ sr}^{-1}$ , or an emission measure  $\text{EM} = 2.75 \text{ cm}^{-6} \text{ pc}$  for gas at  $10^4 \text{ K}$ .

components of foreground emission from the ISM are important (Bennett et al. 1992): 1) bremsstrahlung (or “free-free”) emission from free electrons accelerated by interactions with ions in a plasma, 2) synchrotron emission from relativistic electrons accelerated by magnetic fields, and 3) thermal emission from dust. The  $H\alpha$  images directly trace the free-free component, because ionized gas emits  $H\alpha$  and bremsstrahlung in direct proportion. In addition, the  $H\alpha$  images indirectly trace the thermal emission from that dust associated with the ionized medium.

This paper shows that  $H\alpha$  and  $100\ \mu\text{m}$  emissions are weakly correlated at high galactic latitude. High latitude, filamentary nebulosities have been observed before (Guhathakurta & Cutri 1994, Sandage 1976, and references in each), but verifying the emission to be  $H\alpha$  in particular had not been possible. In fact, Guhathakurta & Tyson (1989) showed that the optically broad-band red color of cirrus is not due to  $H\alpha$  emission, but may be due to luminescence of hydrocarbons. Kogut et al (1996) have shown that multi-frequency radio emissions (commensurate with free-free) are correlated with  $140\ \mu\text{m}$  emission. Broadbent, Haslam, & Osborne (1989) have shown that free-free emission and thermal dust emission are positively correlated at low galactic latitude, i.e. emissions from H II regions.

At low galactic latitudes, there is considerable confusion for optical tracers of gas: where there is gas, there tends to be dust too, and the dust that is emitting at  $100\ \mu\text{m}$ , for example, is absorbing  $H\alpha$  light. Even at high latitudes, where dust opacity is minor (Reynolds 1980), for any integral along a line of sight, the  $100\ \mu\text{m}$  surface brightness is proportional to the density of dust, whereas the  $H\alpha$  surface brightness is proportional to the electron density *squared* (see Section 5). For these reasons, we do not expect a strict proportionality between the  $H\alpha$  and infrared emissions.

Our  $H\alpha$  images provide not absolute surface brightnesses but only relative ones. The same is true of the IRAS images. We do not attempt absolute calibration of the  $H\alpha$  surface brightness because our  $H\alpha$  filter’s 1 nm bandpass is too wide to suppress geocoronal  $H\alpha$ , which is typically a few Rayleighs and varies with time (Broadfoot & Kendall 1968). Fabry-Perot spectroscopy allows absolute calibration of  $H\alpha$  surface brightness, and the infrared has been calibrated by COBE. However, to compare IRAS and  $H\alpha$  images, it suffices to filter out the background in the same way for both images, and that we have done (see Section 3).

## 2. Instrumentation and Observations

The observations were made at the Mt. Laguna Observatory with a wide-field, narrowband imaging camera similar and yet superior to other such cameras (e.g. Bothun & Thompson 1988). We attached it “piggy-back” upon a 1-m telescope, which was used solely for blind pointing and tracking; no acquisition or guiding was necessary. The camera consists of a filter wheel, a 135-mm f/2.8 lens, and a  $2048\times 2048$  pixel CCD. With the 135-mm lens, the  $15\text{-}\mu\text{m}$  pixel spacing corresponds to  $0.38'$ /pixel, and a field of view of  $13^\circ\times 13^\circ$ .

To tune the center wavelength of the 1.0 nm wide (FWHM) H $\alpha$  filter, the filter wheel was thermoelectrically cooled and thermostatically controlled to a precision of 1° C. The temperature was set such that the H $\alpha$  filter’s transmission of zero-velocity H $\alpha$  peaked off the optical axis while maintaining the on-axis transmission to greater than 75% of the peak. At off-axis angles of  $> 4.8^\circ$ , the transmission of zero-velocity H $\alpha$  drops below 50%, so each image is cropped at a radius of  $4.8^\circ$ . Other than cropping, we made no attempt to correct for the radial dependence of the sensitivity to zero-velocity H $\alpha$ . Considering that and other potential errors, we estimate our absolute scaling of H $\alpha$  surface brightness could be in error by as much as a factor of 1.5. Observations of external galaxies show the velocity coverage extends from  $-250$  km/s to  $+250$  km/s.

The backside illuminated CCD has a quantum efficiency at 656.3 nm of 95% (Leach 1996). The sensor is cooled with liquid nitrogen to  $-120^\circ$  C, so for these observations, dark current is negligible. The noise of the readout amplifier is  $9 e^-$  rms, but the integration times were selected so that the readout noise would be negligible compared to the Poisson noise of the sky’s photons.

Forty-eight pairs of exposures were taken over a period of 5 nights, September 21-25, 1995. Each pair consisted of a continuum image followed by an H $\alpha$  image while the telescope turned at the sidereal rate for the duration of the pair. Each continuum image was a 1-minute exposure through a R band filter, except for the first few, which were 2 minutes each (and which had too many saturated stars). Each H $\alpha$  exposure was 20 minutes; the total observing time on-source was 16 hours. The images were dithered; that is, the telescope was repositioned after each pair of images. The dithering pattern was a  $5 \times 5$  grid with  $1^\circ$  spacing, covered almost twice with the 48 image pairs.

We observed the North America nebula and Barnard’s Loop to calibrated the H $\alpha$  surface brightness. These two H II regions have surface brightnesses of 850 R and 153 R (each  $\pm 10\%$ , Reynolds 1980), averaged over  $48'$  diameter fields centered on  $21\text{h}00\text{m}.0 +45^\circ 00'$  [2000] and  $05\text{h}53\text{m}.8 -06^\circ 08'$  [2000].

### 3. Data Reduction

Much of the data reduction is aimed at eliminating stars from the images while preserving the diffuse H $\alpha$  emission. The stars are suppressed in a number of ways: 1) continuum subtraction, 2) flagging pixels that are bright in continuum, 3) flagging pixels at the locations of filter-induced flares near very bright stars, and 4) median filtering with a spatial scale larger than a stellar image.

The CCD bias was determined by overscanning. The relative gain correction for the CCD pixels (the “flat field”) was determined by observing the zenith at sunset in order to minimize gradients and curvatures (Chromey & Hasselbacher 1996). Each continuum image was scaled by a constant and subtracted from the H $\alpha$  images. The constant was empirically-determined based upon stars in each field.

The continuum-subtracted images invariably exhibited a smooth intensity pattern with radial symmetry about the optical axis. The radial pattern may be due to telluric line emission, although it could also be due to the combination of vignetting and inaccuracy of the flat fields. In any event, the circular pattern was removed by fitting and subtracting circular isophotes.

Our experience has been that continuum subtraction is adequate for faint stars, but inadequate for bright stars. Invariably, the two images are not focused identically or they are not registered well enough or both. In the presence of these systematic errors and the increased Poisson noise at the positions of bright stars, it is worthwhile to excise those pixels near bright stars from the data. We flag pixels in the  $H\alpha$  images based upon their respective intensities in the R band images, and flagged pixels are excluded when computing the medians described below.

Each image was median filtered spatially with a  $2^\circ$  diameter ring median filter (Secker 1995). Each median-filtered image was subtracted from its original to eliminate large scale intensity variation due to the variation in airmass across the field, residual inaccuracies in flat fielding, or the occasional telluric cirrus cloud. To check that this procedure was not eliminating real emission from the Milky Way, we also reduced the data without this median filtering step, but instead substituted fitting and subtracting a plane of intensity. The two methods give similar results.

The images were registered automatically to a common coordinate system, using a few dozen SAO stars on each image to determine the appropriate shift, expansion, rotation, and distortion. The 48 registered images were combined by averaging them pixel by pixel, while excluding flagged pixels. Also, an iterative procedure eliminated those individual pixel values that were further than  $2\sigma$  from the median of the other values for that particular pixel. Finally, a ring median filter of radius  $2.3'$  was applied, and then the image was convolved with a circular Gaussian of width  $\sigma = 1.5'$ .

#### 4. Results

The  $H\alpha$  image (Figure 1) appears similar to the corresponding area of sky observed by IRAS at  $100\ \mu\text{m}$  (Figure 2). We have inscribed boxes in Figures 1 and 2 that contain the two most apparent similarities: 1) at left, a filled arc of  $100\ \mu\text{m}$  emission, enveloped by an arc of  $H\alpha$  emission, and 2) at center-top, a potato-shaped outline in both  $100\ \mu\text{m}$  and  $H\alpha$  emission.<sup>3</sup>

To quantify the association between the  $H\alpha$  and  $100\ \mu\text{m}$  emissions, we evaluated their (Pearson) correlation coefficient,  $\rho = +0.115$ , over the central  $8.5^\circ \times 8.5^\circ$  subregions of the  $13^\circ \times 13^\circ$  images. The subregion was selected because the effective observing time is less near all edges of the  $H\alpha$  mosaic and because residual, circular artifacts of the mosaicing process are apparent near the western edge.

---

<sup>3</sup>A “movie” that “blinks” the two  $H\alpha$  and  $100\ \mu\text{m}$  images is available from the author.

We also correlated the H $\alpha$  image with 36 controls. The controls are 100  $\mu\text{m}$  IRAS images from “random” but statistically similar directions on the sky, centered at galactic coordinates  $b = \pm 67^\circ$ ,  $l = 1^\circ, 21^\circ, \dots, 341^\circ$ . Each control was created and processed like the image in Figure 2. The controls should be uncorrelated with the H $\alpha$  image (i.e. the expectation value,  $E(\rho) = 0$ ), so they provide a standard by which to judge the validity of our measured correlation. The distribution of correlation coefficients of the 36 controls is approximately Gaussian, with  $\mu = -0.017$  and  $\sigma = 0.041$  (see Figure 3).

The measured correlation coefficient ( $\rho = +0.115$ ) is statistically significant from zero by  $+2.8\sigma$ . From the controls we can conclude with  $\sim 95\%$  confidence<sup>4</sup> that  $\rho \neq 0$ , but we should not immediately conclude that  $\rho = +0.115 \pm 0.041$ . Mathematically, we expect  $\rho$  to be larger than  $+0.115$  because noise in the data tends to reduce  $|\rho|$  from its true value. Physically, we expect  $\rho$  to be larger or smaller for various directions on the sky. For example, in the boxes of Figures 1 and 2, which were inscribed because the emissions within them looked similar,  $\rho = +0.150$ .

The bias of  $\rho$  due to noise in the two images can be estimated, and it is not large. We let  $\sigma_i^2$  equal the variance of the infrared intensity and we let  $\sigma_h^2$  equal the variance of the H $\alpha$  intensity, both as measured over the inner  $8.5^\circ \times 8.5^\circ$  subregions. The  $\sigma_i^2$  and  $\sigma_h^2$  each include both genuine variation of emission and random noise. We evaluate the noise variances in each image,  $\eta_i^2$  and  $\eta_h^2$ , by computing the average of the variances in small regions apparently lacking emission. If the ratios  $\sigma_i^2/\eta_i^2$  and  $\sigma_h^2/\eta_h^2$  are both large compared to unity, the bias is small and more precise estimates of the noise are not warranted. The measured values are  $\sigma_i/\eta_i = 2.4$  and  $\sigma_h/\eta_h = 2.6$ . It can be shown that the ratio of the true to the observed (Pearson) correlation coefficients is

$$\frac{\rho_{\text{true}}}{\rho_{\text{obs}}} = \sqrt{\frac{\sigma_i^2}{\sigma_i^2 - \eta_i^2}} \sqrt{\frac{\sigma_h^2}{\sigma_h^2 - \eta_h^2}}, \quad (1)$$

which in this case is 1.19 and is smaller than the fractional uncertainties of both the statistical variation of  $\rho$  estimated from the controls and the spatial variation evident from the value of  $\rho = +0.150$  of the alternative subregion. Accounting for the bias of noise, we estimate  $\rho = +0.14 \pm 0.04$ .

Having established that the 100  $\mu\text{m}$  and H $\alpha$  emissions are weakly correlated, we evaluate the ratio of the two correlated emissions by a linear fit of the form,  $I(100 \mu\text{m}) = a I(\text{H}\alpha) + b$ , to the data within the central  $8.5^\circ \times 8.5^\circ$  subregions of the two images. The slope “a” is of interest; the value “b” is not, because the zero points of both the 100  $\mu\text{m}$  intensity and the H $\alpha$  intensity are arbitrary. Because both the 100  $\mu\text{m}$  and H $\alpha$  emissions have substantial observational errors, ordinary least squares fitting is invalid.<sup>5</sup> We fit the data by two methods as described below. Both

---

<sup>4</sup>That 2 of 36 controls share the same bin in Figure 3 as the true correlation coefficient indicates a  $\sim 5\%$  likelihood that the two emissions are uncorrelated ( $\rho = 0$ ), i.e. that the measured correlation is due solely to chance.

<sup>5</sup>In this context “ordinary” least squares refers to fitting a “dependent” (noisy) variable Y against an “independent” (noise-free) variable X.

methods allow for errors in each of the observed quantities.

The first method is based upon the work of Feigelson & Babu 1992.<sup>6</sup> It yields a value for the slope  $a = 1.2(\pm 0.12)$  MJy sr<sup>-1</sup> R<sup>-1</sup>, under the assumption of additive Gaussian errors of zero mean and variances of  $(0.17 \text{ MJy sr}^{-1})^2$  and  $(0.077 \text{ R})^2$ , for the 100  $\mu\text{m}$  and H $\alpha$  emissions, respectively. We determined the variance of the H $\alpha$  emission,  $(0.077 \text{ R})^2$ , from an ensemble of 1-dimensional Gaussian fits to the bivariate distribution of 100  $\mu\text{m}$  and H $\alpha$  emissions by rows; the variance of the 100  $\mu\text{m}$  emission was determined similarly, but by columns (cf. Figure 4). Note that those variances include real (but uncorrelated) emission in addition to detector and shot noise; the uncorrelated emissions act as approximately Gaussian “errors” with respect to the correlated components of the emissions. We consider the formal error ( $\sigma_a = 0.12 \text{ MJy sr}^{-1} \text{ R}^{-1}$ ) to be a lower limit of the true error. To investigate empirically the reliability of the slope estimate, we performed the same analysis separately on the four quadrants of the central  $8.5^\circ \times 8.5^\circ$  subregion. The slopes so measured were 1.5, 1.4, 1.3, and 0.6 MJy sr<sup>-1</sup> R<sup>-1</sup> for the NW, NE, SW, and SE quadrants, respectively.

The second method is a simplification of the “BCES” method of Akritas & Bershady 1996. BCES refers to “bivariate correlated errors and intrinsic scatter”; our simplification is to assume that the observational errors of the 100  $\mu\text{m}$  and H $\alpha$  emissions are uncorrelated. We evaluate the observational errors by examining small regions apparently lacking emission. The standard deviations so measured are 0.07 MJy sr<sup>-1</sup> and 0.04 R, for the 100  $\mu\text{m}$  and H $\alpha$  emissions respectively. The BCES bisector slope (see Akritas & Bershady 1996), evaluated over the central  $8.5^\circ \times 8.5^\circ$  subregion, yields the same slope as the first fitting method,  $a = 1.2 \text{ MJy sr}^{-1} \text{ R}^{-1}$ . Likewise, the BCES bisector slopes for the NW, NE, SW, and SE quadrants are 1.68, 1.31, 1.16, and 1.53 MJy sr<sup>-1</sup> R<sup>-1</sup>, respectively.

The result of averaging the 8 slopes from the four quadrants and the two methods is  $a = 1.26_{-0.32}^{+0.45} \text{ MJy sr}^{-1} \text{ R}^{-1}$ . The mean value given is a vector average (i.e.  $\langle a \rangle = \tan(\langle \arctan(a_i) \rangle)$ ,  $i = 1, \dots, 8$ ). The excursions (+0.45 and -0.32) describe the  $1\sigma$  dispersion of the 8 slopes, also calculated vectorially, not arithmetically. Additional observations are required to determine if the dispersion of slopes is statistical or intrinsic to the ISM.

The brightest object in the H $\alpha$  image has no counterpart at 100  $\mu\text{m}$ , illustrating that the correlation between 100  $\mu\text{m}$  and H $\alpha$  emissions is not true in general. To the contrary, additional observations at lower galactic latitudes ( $|b| < 30^\circ$ ) and of less sensitivity show many H $\alpha$  features with no infrared counterparts (McCullough 1997). Those additional images also show H $\alpha$ –infrared correlations, both positive and negative. At the lower Galactic latitudes, there is considerable confusion.

The brightest object in Figure 1 may be associated with the Magellanic Stream; it lies

---

<sup>6</sup>Note that their variable  $l = \sigma_y^2/\sigma_x^2$ , not  $\sigma_x^2/\sigma_y^2$  as originally printed.

between two H I peaks of MS IV (Cohen 1982) and its long axis is parallel to the Magellanic Stream. If so, it is the brightest H $\alpha$  emission from the Magellanic Stream (cf. Weiner & Williams 1996, Weiner 1996). However, it might be simply a density enhancement in the ISM unrelated to the Magellanic Stream. The critical test is to measure its velocity.

## 5. Discussion

The H $\alpha$  light we observe could be from either a reflection nebula or an emission nebula, or both. In this Section we show that the reflection component is expected to be small compared to the emission component.

In the case of a reflection nebula, the surface brightness of the H $\alpha$  light is proportional to the product of the surface emissivity in H $\alpha$  of the disk of the Milky Way and the dust column density along the line of sight. Using canonical values for the surface emissivity, the ratio of dust to gas, and the dust’s scattering cross section and phase function, Jura (1979) predicts the surface brightness of the H $\alpha$  light  $I_\alpha$  (in Rayleighs) backscattered from dust:

$$I_\alpha = 0.10 \frac{N_H}{10^{20} \text{cm}^{-2}}, \quad (2)$$

where  $N_H$  is the total hydrogen column density.

In the case of an emission nebula, the surface brightness of the H $\alpha$  light  $I_\alpha$  (in Rayleighs) is proportional to the emission measure (Reynolds 1992):

$$I_\alpha = 0.36 T_4^{-0.92} \text{EM}, \quad (3)$$

where  $T_4$  is the electron temperature in units of  $10^4$  K. In the warm ionized medium of the ISM,  $T_4 \approx 0.8$  (Reynolds 1992). The emission measure  $\text{EM} = \int n_e n_p dl \approx \int n_e^2 dl$  has units  $\text{cm}^{-6}\text{-pc}$ . The region is assumed to be optically thick to Lyman lines (a.k.a. Case B), and extinction is ignored, but otherwise, equation 3 is derived directly from the fundamental physics of recombination.

From the emission measures and dispersion measures along the high-latitude lines of sight to a few globular clusters containing pulsars, Reynolds (1991a) shows that the density of high latitude ionized gas, where it exists<sup>7</sup> is  $\sim 0.08 \text{ cm}^{-3}$  and the ratio of the ionized hydrogen column density to the total hydrogen column density ranges from 0.2 to 0.4 (Reynolds 1991b), with an average of 0.27 for the five lines of sight.

Combining the emission and reflection contributions to the H $\alpha$  surface brightness using the above values from the literature, we find

$$I_\alpha = \left( 11.7 T_4^{-0.92} n_e \frac{N_{\text{H}^+}}{N_H} + 0.10 \right) \frac{N_H}{10^{20} \text{cm}^{-2}},$$

---

<sup>7</sup>Reynolds estimates that the ionized gas fills  $\sim 20\%$  of the volume.

$$= (0.31 + 0.10) \frac{N_{\text{H}}}{10^{20} \text{cm}^{-2}}, \quad (4)$$

where we have expressed the EM as a product of the volume density,  $n_e$ , and the ionized hydrogen column density,  $N_{\text{H}^+}$ , by approximating  $\int n_e n_p dl \approx n_e \int n_{\text{H}^+} dl$ . The latter approximation is valid if hydrogen is the dominant ion and if the electron volume density is bimodal, i.e. either  $n_e$  is  $0.08 \text{ cm}^{-3}$  or it is zero.

Equation 4 predicts the emission component to be  $\sim 3$  times greater than the backscattered component. The backscattering component will be less than a third of the emission component if the gas is either denser or more highly ionized than we have assumed. Reynolds et al (1973) estimate the ratio of backscattered to total  $\text{H}\alpha$  light to be 0.1 ( $-0.1, +0.2$ ) toward a few Lynds nebulae.

It is well known that dust and neutral hydrogen are positively correlated in general (Boulanger & Perault 1988), but is that true in this region? The three H I maps of highest resolution and sensitivity (Hartmann 1994, Heiles & Habing 1974, Cohen 1982) are inadequate to allow us to answer this question because the beams are too large ( $0.5^\circ$  FWHM) and the sensitivity is too poor (the r.m.s. is equivalent to  $N_{\text{H}} \approx 1$  to a few times  $10^{19} \text{ cm}^{-2}$ ). The *peak*  $100 \mu\text{m}$  emission,  $\sim 0.5 \text{ MJy sr}^{-1}$  above the background, corresponds to a *peak* H I column density of  $6 \times 10^{19} \text{ cm}^{-2}$ , assuming  $I_{100} = 0.85 N_{\text{H}} / 10^{20} \text{ cm}^{-2} \text{ MJy sr}^{-1}$  (Boulanger & Perault 1988). Nevertheless, we analyzed the H I column density data of Heiles & Habing (1974) exactly as we did the  $\text{H}\alpha$  data above and found no statistically significant correlation with the  $100 \mu\text{m}$  data.<sup>8</sup> The H I&infrared correlation coefficient is  $-0.119$ , which corresponds to  $1.5\sigma$  less than zero ( $\sigma = 0.078$  is evaluated as before using thirty six  $100 \mu\text{m}$  controls). The anticorrelation of H I&infrared in the same region where  $\text{H}\alpha$ &infrared is positively correlated is intriguing, but it is not statistically significant. The anticorrelation also is opposite in sign to the firmly established results of Boulanger & Perault (1988).

In Section 4 the slope of the correlated components of the  $100 \mu\text{m}$  and  $\text{H}\alpha$  emissions is estimated to be  $1.26_{-0.32}^{+0.45} \text{ MJy sr}^{-1} \text{ R}^{-1}$ . From 4 years of COBE data, Kogut et al. (1996) determine the slope of the correlated components of the antenna temperature  $T_{\text{A}}$  of the DMR at 31.5 GHz with respect to the  $140 \mu\text{m}$  surface brightness  $I_{140}$  measured with DIRBE:  $T_{\text{A}}/I_{140} = 6.37(\pm 1.52) \mu\text{K}(\text{MJy sr}^{-1})^{-1}$ . In so far as free-free emission dominates thermal dust emission at 31.5 GHz, the slope  $6.37(\pm 1.52) \mu\text{K}(\text{MJy sr}^{-1})^{-1}$  corresponds<sup>9</sup> to a ratio  $I_{140}/I_{\text{H}\alpha} = 0.90_{-0.17}^{+0.29} \text{ MJy sr}^{-1} \text{ R}^{-1}$ , which is similar to the  $I_{100}/I_{\text{H}\alpha}$  ratio derived in this work. On the  $\sim 7^\circ$  angular scale of DMR, Kogut et al. 1996 conclude that more than one third of (and perhaps “the bulk of”) the free-free emission must be from that component correlated with  $140 \mu\text{m}$  emission. At much smaller angular scales, the bulk of the  $\text{H}\alpha$  emission is not correlated with

---

<sup>8</sup>The data of Cohen 1982 exist only on 8-hole paper tape, and the data of Hartmann 1994 were not yet publicly available in machine readable form when this paper was written.

<sup>9</sup>See e.g. Bennett et al. 1992 equation 4.



100  $\mu\text{m}$  emission (Section 4); thus it appears that the correlation between ionized gas and dust emissions increases with increasing angular scale.

## 6. Summary

An  $\text{H}\alpha$  image of a  $13^\circ \times 13^\circ$  region at  $(l,b) = (71^\circ, -67^\circ)$  shows structure  $\sim 10$  times fainter than the  $12^\circ \times 10^\circ$  region of sky at  $(l,b) = (144^\circ, -21^\circ)$  previously observed by Reynolds (1980). The new image gives a preliminary view of the sky over many degrees at unprecedented sensitivity. The new  $\text{H}\alpha$  image weakly resembles the 100  $\mu\text{m}$  IRAS image; a point-by-point comparison of the two shows a positive correlation ( $\rho = +0.14 \pm 0.04$ ); and comparison with COBE data indicates that the correlation coefficient increases with increasing angular scale. The slope of the correlated components of the 100  $\mu\text{m}$  and  $\text{H}\alpha$  emissions is  $1.26_{-0.32}^{+0.45} \text{ MJy sr}^{-1} \text{ R}^{-1}$ .

An important extension of this work (already underway by many investigators) will be to image the  $\text{H}\alpha$  emission over much of the sky. An all-sky  $\text{H}\alpha$  image may prove critical to distinguishing the Galactic foreground from the cosmic background at the precision necessary to determine cosmological parameters.

Jeremy Hicks assisted with the observing. Bob Leach made the CCD camera. We appreciate discussions with John Gaustad, Carl Heiles, Margaret Meixner, William Reach, Ron Reynolds, and Dave Van Buren. We thank Ben Weiner for providing data in advance of publication.

## REFERENCES

- Akritas, M.G. & Bershad, M.A. 1996, *Astrophys. J.*, 470, 706  
Bennett, C. L, et al. 1992, *Astrophys. J.*, 396, L7  
Bothun, G. D, and Thompson, I. A. 1988, *Astron. J.*, 96, 877  
Boulanger, F. & Perault, M. 1988, *Astrophys. J.*, 330, 964  
Broadbent, Haslam, & Osborne 1989, *MNRAS*, 237, 381  
Broadfoot, A.L., & Kendall, K.R. 1968, *JGR*, 73, 426  
Chromey, F.R. and Hasselbacher, D. 1996, *PASP*, 108, 944  
Cohen, R.J. 1982, *MNRAS*, 199, 281  
Feigelson, E.D. & Babu, G.J. 1992, *Astrophys. J.*, 397, 55

- Guhathakurta, P. & Cutri, R.M. 1994, in ASP Conf. Series Vol 58, “The First Symposium on the Infrared Cirrus and Diffuse Interstellar Clouds,” Cutri & Latter, eds., p. 34-44.
- Guhathakurta, P. & Tyson, J.A. 1989, *Astrophys. J.*, 346, 773
- Hartmann, D. 1994, Ph.D. Thesis, University in Leiden
- Harwit, M. 1981, *Cosmic Discovery* (New York:Basic Books)
- Heiles, C. & Habing, H. J. 1974, *A&A Suppl. Ser.* 14, 1
- Kogut et al. 1996, *Astrophys. J. Letters*, 464, L5
- Kulkarni S.R. & Heiles, C. 1987, in *Interstellar Processes*, eds. D.J. Hollenbach, H.A. Thronson, Jr., (Dordrecht: Kluwer), 87
- Leach R. 1996, private communication
- Lo, F.G. et al. 1984, *Astrophys. J. Letters*, 278, L19
- McCullough, P.R. 1996, *IAU Symp.* 179, “New Horizons from Multi-Wavelength Sky Surveys,” Kluwer
- Reynolds, R. J., Scherb, F. and Roesler, F.L. 1973, *Astrophys. J.*, 185, 869
- Reynolds, R. J. 1980, *Astrophys. J.*, 236, 153
- Reynolds, R. J. 1988, *Astrophys. J.*, 333, 341
- Reynolds, R. J. 1991a, *Astrophys. J. Letters*, 372, L17
- Reynolds, R. J. 1991b, in *IAU Symp.* 144, *The Interstellar Disk-Halo Connection in Galaxies*, ed. H. Bloemen (Dordrecht: Kluwer), 67
- Reynolds, R. J. 1992, *Astrophys. J. Letters*, 392, L35
- Sandage, A. 1976, *Astron. J.*, 81, 954
- Secker, J. 1995, *PASP*, 107, 496
- Weiner, B.J. & Williams, T.B. 1996, *Astron. J.*, 111, 1156
- Weiner, B.J., private communication.



Fig. 1.— This  $H\alpha$  image is  $13^\circ$  on a side and shows features as faint as 0.2 Rayleighs. The triangular object near the center is the brightest object in the field, at 0.6 R. The inscribed box contains two  $H\alpha$  emission features associated with IRAS  $100\mu\text{m}$  emission: the arc at left and the potato-shaped outline at top-center (cf. Figure 2). The center of the image is  $23\text{h}40\text{m}00\text{s} -12^\circ00'00''$  [2000],  $(l,b) = (71^\circ.5, -67^\circ.4)$ . North is up and East is to the left. The Galactic plane is toward the upper-right (NW).

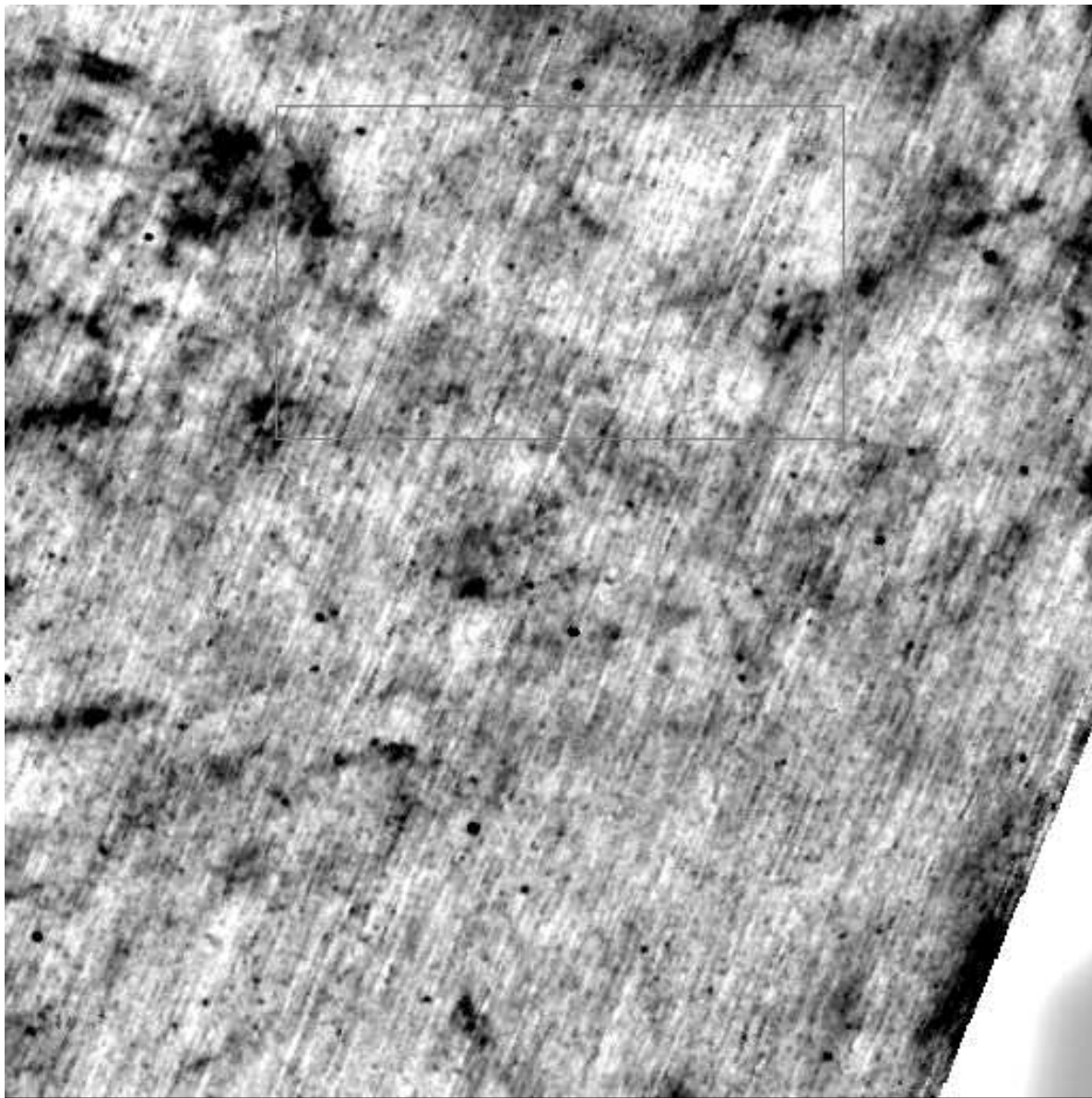


Fig. 2.— This IRAS  $100\mu\text{m}$  image shows the same region as Figure 1. Because of its proximity to the ecliptic, this field is one of the so-called “reject” fields of IRAS. To reduce variations on large angular scales, a  $2^\circ$  diameter ring-median filtered version of this image was subtracted from the original. The same filtering was applied to Figure 1.

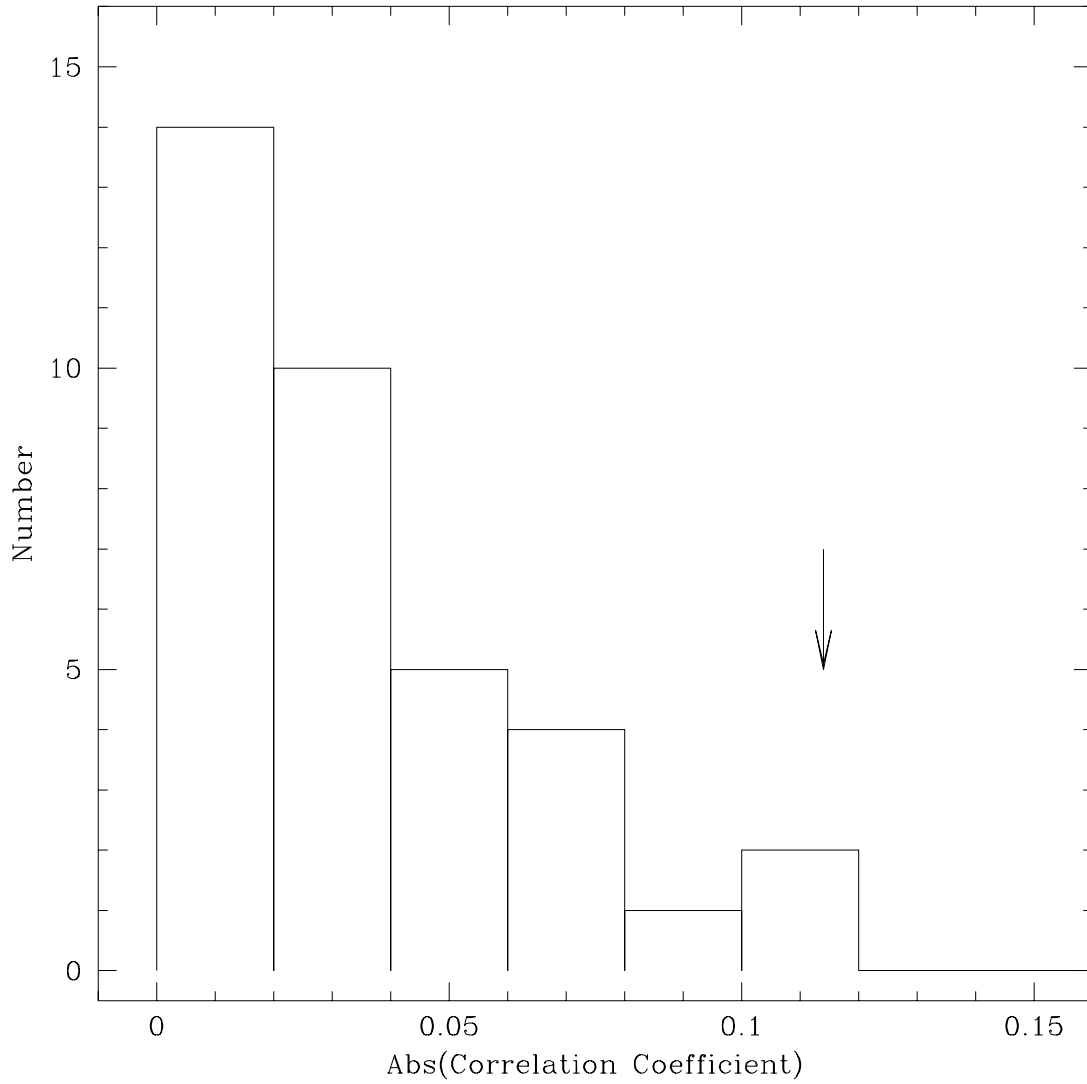


Fig. 3.— This histogram of the absolute values of the correlation coefficients of 36 controls shows that the correlation coefficient of the H $\alpha$  and 100 $\mu$ m emissions in Figures 1 and 2, +0.115 (arrow), is statistically significant at  $3\sigma$ .

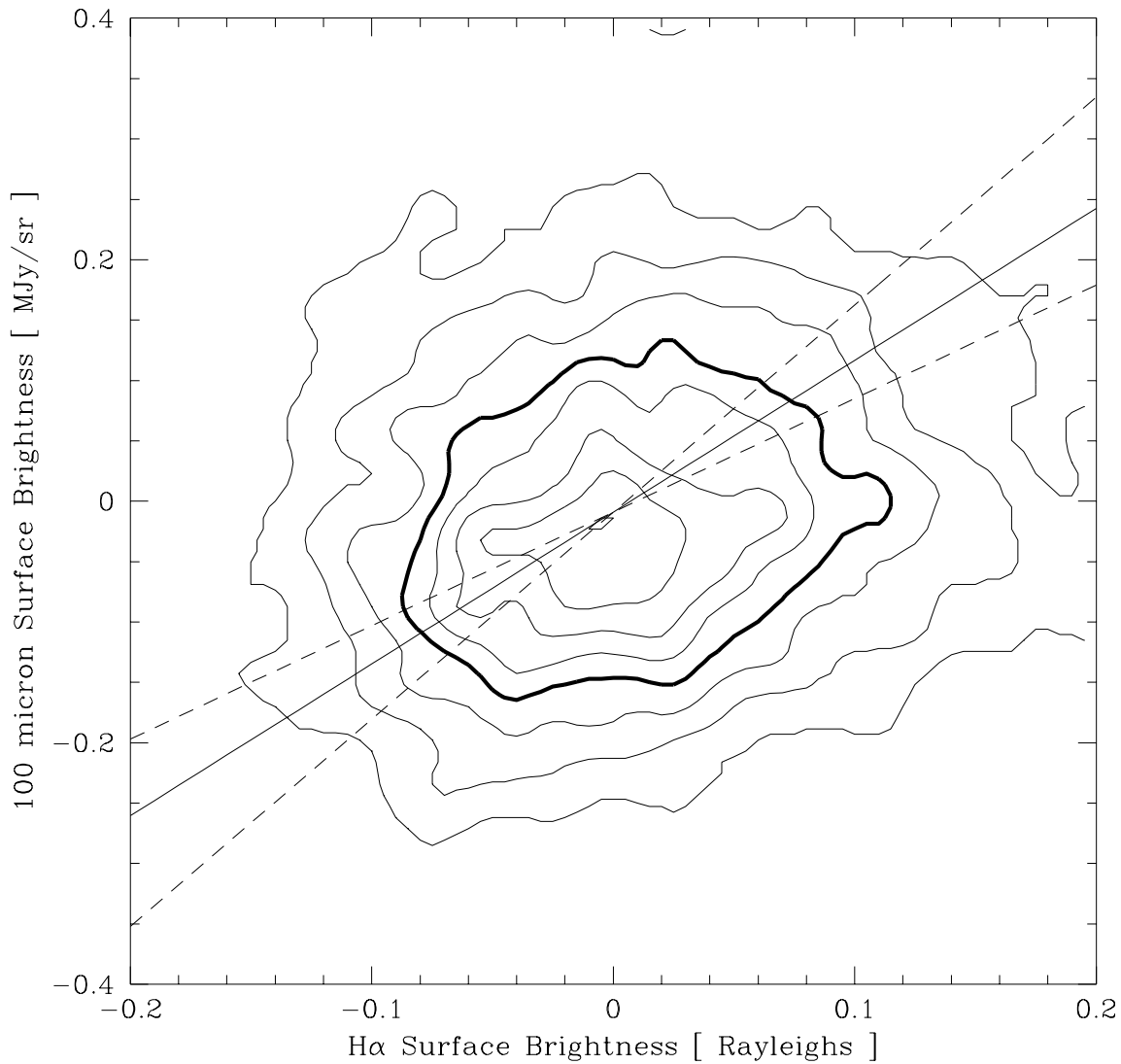


Fig. 4.— The  $100\mu\text{m}$  versus  $\text{H}\alpha$  bivariate distribution is plotted (contours); the best fit line (solid) and lines with  $\pm 1\sigma$  deviations of the slope (dashed) are superimposed. The contours are linearly spaced at intervals of 12.5%, 25%, ... of the peak; the 50% contour is bold. The data are from the central  $8.5^\circ \times 8.5^\circ$  subregions of the  $13^\circ \times 13^\circ$  images in Figures 1 and 2.